EBV Encoded miRNA BART8-3p Drives Radioresistance-Associated Metastasis in Nasopharyngeal Carcinoma

Xiaohan Zhou
Southern Medical University Nanfang Hospital
Yanling Lin
Southern Medical University Nanfang Hospital
Yuting Chen
Southern Medical University Nanfang Hospital
Lingzhi Wang
Southern Medical University Nanfang Hospital
Jinrong Liao
Southern Medical University Nanfang Hospital
Hanyi Zeng
Southern Medical University Nanfang Hospital
Wenxiao Luo
Southern Medical University Nanfang Hospital
Dehua Wu
Southern Medical University Nanfang Hospital
Longmei Cai (clm520@i.smu.edu.cn)
Southern Medical University Nanfang Hospital

Research

Keywords: Epstein-Barr virus, miR-BART8-3p, nasopharyngeal carcinoma, radioresistance, metastasis

Posted Date: July 23rd, 2020

DOI: https://doi.org/10.21203/rs.3.rs-46774/v1

Abstract

Background: Radiotherapy plays an important role in the treatment of nasopharyngeal carcinoma (NPC), however, 20 % of patients with NPC exhibit unusual radioresistance. Patients with radioresistance are at risk of recurrence, so it is imperative to explore the mechanism of resistance to radiotherapy. In the past, studies on the mechanism of radioresistance have been restricted to DNA damage and related cell cycle remodeling or apoptosis. So far, no studies have explored the relationship between radioresistance and metastasis.

Methods: We analyzed the metastasis rate of patients with recurrent NPC and that of patients with primary NPC. Constructing an acquired radioresistant NPC cell line and detect their metastatic ability in vivo and in vitro. RNA-deep sequencing was performed to predict the targeted host genes of EBV-miR-BART8-3p. Western blotting, real-time PCR and immunochemistry were conducted to investigate the relationship of clinicopathologic features and EBV-miR-BART8-3p or PAG1.

Results: Through the analysis of clinical samples, we observed that the metastasis rate of recurrent NPC was much higher than that of primary patients. In vitro and in vivo experiments showed that NPC cells with acquired radioresistance exhibited a stronger ability for invasion and metastasis. Mechanistically, we found that the Epstein–Barr virus (EBV)-encoded miRNA BART8-3p was increased in patients with NPC and its expression was positively correlated with adverse prognostic factors, such as radioresistance. Besides, miR-BART8-3p promoted the epithelial-mesenchymal transition (EMT), invasion, and metastasis of radioresistant NPC cells by targeting and inhibiting their *PAG1* host gene.

Conclusion: These results demonstrated a correlation between radioresistance and metastasis in NPC, which depended on the elevated levels of the EBV-encoded miRNA BART8-3p and the inhibition of the PAG1 host gene. These findings suggested a novel role for EBV-miR-BART8-3p and PAG1 in recurrence NPC and highlighted their potential value as prognostic indicators or therapeutic targets.

Background

Nasopharyngeal carcinoma (NPC) is remarkable for its distinct racial and geographic distributions, being a common malignant tumor in Southeast Asia, North Africa, Alaska, and the Mediterranean basin [1]. Although radiotherapy is the preferred treatment for NPC, radioresistance is an important problem in the treatment of NPC. Recurrence and metastasis of NPC due to radioresistance are known to occur in 20% of the total number of patients [2]. Both recurrence and metastasis are important signs of poor prognosis. In particular, it has been reported that 20% to 30% of relapsed patients have distant metastatic tumors [2, 3]. Compared with patients with better local control, patients with NPC with local recurrence are known to be more likely to have secondary distant metastasis [4, 5]. Therefore, a better understanding of the relationship underlying radioresistance and metastasis of NPC is likely to improve survival and facilitate the design of novel therapeutic strategies for NPC.

Postradiotherapy plasma Epstein–Barr virus (EBV) DNA is known to play an important role in the risk stratification of NPC [6], suggesting that EBV viral encoding products might play an important role in the metastasis of NPC. Noted, EBV is the first human virus found to encode microRNAs (miRNAs). To date, a total of 25 EBV-miR precursors containing 48 mature miRNAs have been identified within 2 regions of the EBV genome. Analysis of the results comparing the miRNA microarray of NPC with that of normal nasopharyngeal (NP) tissues revealed that EBV-miR-BARTs were superior among all differentially expressed miRNAs [7]. Respectively, the mechanism of EBV-miR-BARTs in the radioresistance and metastasis of nasopharyngeal carcinoma has been reported, whereas the bridge function of EBV-miR-BARTs in the radioresistance associated metastasis of NPC remain elusive. In this study, we were interested in the role of viral and cellular miRNAs in the tumor radioresistance-associated metastasis and their clinical significance in NPC, in order to identify potential targets for improving the prognosis of recurrent NPC (rNPC).

In this study, using in vivo and in vitro experiments, we confirmed that NPC radioresistant cell lines were prone to metastasis. We further found that EBV-miR-BART8-3p was highly expressed in radioresistant NPC and closely associated with metastatic features of NPC. The underlying molecular mechanisms by which EBV-miR-BART8 caused tumor metastasis were revealed to involve the direct targeting of the major tumor suppressor phosphoprotein membrane anchor with glycosphingolipid microdomains 1 (*PAG1*), and promotion of its combination with vimentin, which induced epithelial–mesenchymal transition (EMT). Our findings provided new insights into the mechanisms of the EBV-regulated radioresistance in NPC and advocate for the development of clinical intervention strategies for NPC.

Methods

Cell culture

Two EBV-negative NPC cell lines (5-8F and HONE1) and 1 EBV-positive NPC cell line (C666-1) were kindly provided by Professor Musheng Zeng, Sun Yat-sen University Cancer Center of Guangzhou, China. One EBV-positive NPC cell line (HNE1-EBV) was kindly provided by Professor S.-W. Tsao, University of Hong Kong, China. HEK293T cells were obtained from Cancer Research Institute Southern Medical University of Guangzhou, China. All cell lines were cultured in RPMI-1640 (Invitrogen,Carlsbad, CA, USA) supplemented with 10 % newborn cow serum (NCS; Hyclone, Invitrogen). All cells were maintained at 37 °C with 5 % CO_2.

Patients and specimens

A cohort containing 62 NPC specimens with TNM staging was collected for the association analysis of the expression of EBV-miR-BART8 with pathological and clinical data (Supplementary Table 1-2). All clinical samples used for immunohistochemistry (IHC) analysis of the expression of *PAG1* were collected from the Nanfang Hospital of Southern Medical University, Guangzhou, China (Supplementary Table 3).The biopsy specimens of the validation set were obtained from a clinical trial conducted by our study

group (Clinical Trials.gov no.NCT01171235). Tumor stage was scored according to the American Joint Committee on Cancer staging system (7th edition).

Establishment of radioresistant cells

C666-1 cells were exposed to 6 Gy X-rays once every 2 wk for a total of 5 times (cumulative dose: 30 Gy), yielding C666-1R cells. After the final exposure, cells were cultured under normal conditions for 4 wk.

Colony formation assay for radiosensitivity and irradiation

Colony formation assays were performed to assess the radiosensitivity of cells after IR. Suspensions containing 200, 400, 800, 1600, and 3200 cells were seeded into 6-well plates and exposed to 0, 2, 4, 6, or 8 Gy (2 Gy perfraction), respectively, using a 6 MV X-ray beam from an Elekta linear accelerator (Precise 1120; Elekta Instrument AB, Stockholm, Sweden) at a dose rate of 220 cGy/min. Cells were incubated for 14 d until colony appearance. Colonies were fixed for 15 min with carbinol (Huada, Guangdong, China) and stained for 30 min with 0.1 % Giemsa (AppliChem, Darmstadt, Germany). Colonies containing >50 cells were counted.

Transwell migration and Boyden chamber invasion assays

For the transwell migration assay, 10^5 cells in 100 mL serum-free RPMI-1640 media were triplicate seeded in each fibronectin-coated polycarbonate membrane insert in a transwell apparatus (Corning, Shanghai, China). Consecutively, 600 mL of RPMI-1640 supplemented with 10 % NCS was added to the bottom chamber. Both C666-1 and C666-1R cells were incubated at 37 °C with 5 % CO_2 for 8 h. Concomitantly, 5-8F, HONE1, and HNE1-EBV cells were incubated for 8, 12, and 8 h, respectively. Cells adhered on the lower surface were fixed with 100 % methanol (Huada) at 25 °C for 15 min and stained with hematoxylin (Macklin, Shanghai, China) for 15 min. Cell numbers in 6 predetermined fields in each replicate were counted under the microscope (NiKon ECLIPSE 80i system,NiKon, Shanghai, China). All assays were independently repeated at least 3 times. Cell invasion assays were performed similar to the migration assay except that the transwell membrane was precoated with 24 mg/mL Matrigel (R&D Systems, Minn, USA).

Lentiviral construction and transduction

Lentiviral particles containing the GV209 expression vector encoding 282-nt of the pri-EBV-miR-BART8 precursor that produces both BART8-5p and BART8-3p (H1-miRNA-CMV-EGFP-BART8), as well as randomized flanking sequence control (H1-miRNA-CMV-EGFP-mock) were purchased from GeneChem (Shanghai, China) and transduced into NPC cells following the manufacturer's instructions. Then, puromycin (Genechem, Shanghai, China) was added to the medium at a final concentration of 3 μg/mL for a 5 d selection.

Animal experiments

Animal experiments were approved by the Ethical Committee for Animal Research of Southern Medical University (protocol number: NFYY-2018-76) and conducted based on the state guidelines from the Ministry of Science and Technology of China. All nude mice (4-6 wk old, male) were purchased from the Central Animal Facility of Southern Medical University. The in vivo metastasis model was established by tail vein injection. Briefly, 1×10^6 NPC cells were suspended in 100 μL serum-free 1640 medium and injected into the tail vein of nude mice (10 mice in each group). Accordingly, 6 wk later, whole bodies, and freshly dissected internal organs, including lungs and livers were collected for fluorescence imaging with the LT-9MACIMSYSPLUS whole-body imaging system (Encinitas, CA, USA). Organs were fixed in 4 % paraformaldehyde (Macklin) for 48 h and transferred to gradient ethanol (Huada). Then, organs were embedded in paraffin (Shitai, Jiangsu, China), sectioned using a Leica RM2235 microtome (Leica Biosystems, Weizler, Germany) and processed for histological examinations.

Immunohistochemistry staining

Paraffin sections prepared from patients were applied to IHC staining for the detection of the levels of PAG1 protein, using the indirect streptavidin-peroxidase method. All antibodies used for IHC are listed in Supplementary Table 4. The intensity of immunostaining was scored as weak (1), medium (2), and strong (3). The extent of staining, defined as the percentage of positive staining cells, was scored as 1 (≤25 %), 2 (26–50 %), 3 (51–75 %), and 4 (>75 %). An overall expression score, ranging from 0 to 7, was obtained by adding the score of the intensity and that of the extent of staining. The final staining score was given as low expression (overall score of 1–4), or high expression (overall score of 4-7).

Wound scratch assay

Cells (5×10^5) were seeded in a 6-well culture dish and grown to 90 % confluence. A single wound was made in the center of the cell monolayer and cell debris was removed by washing twice with PBS (Invitrogen). Complete medium was added and 5-8F or HONE1 cells were allowed to migrate into the clearing area for 24 or 12 h, respectively. Wound closure areas were visualized under an inverted microscope with a 100× magnification, and the migrated areas were counted.

Immunofluorescence assays

Cells were cultured on coverslips overnight, fixed with 4 % formaldehyde in PBS for 15 min at 4 °C and then permeabilized with 0.5 % Triton-X-100 (Beyotime, Shanghai, China) in PBS for 30 min. Subsequently, cells were blocked for nonspecific binding with 5 % milk in TBS (Invitrogen) and Tween-20 (Santa Cruz Biotechnology, Delaware, CA, USA) (TBST) at 25 °C for 30 min, and then incubated with E-cadherin, vimentin, PAG1, or HA antibodies (Supplementary Table 4) at 4 °C overnight. Consecutively, cells were incubated with Alexa Fluor 488 goat anti-rabbit IgG (1:500, Proteintech, Rosemount, IL, USA) and Alexa Fluor 647 goat anti-mouse IgG (1:500, Proteintech) at 37 °C for 1 h. Coverslips were mounted on slides using anti-fade mounting medium with DAPI (Invitrogen). Accordingly, IF images were acquired on an OLYMPUS confocal micrograph system, and analyzed using the FV10-ASW1.7 viewer software (Olympus, Japan).

RNA oligos and cell transfection

The control mimic, miR-BART8-3p mimic, control inhibitor, and miR-BART8-3p inhibitor were synthesized by Integrated DNA Technology (GenePharma, Suzhou, China) (Supplementary Table 5). The culture medium was changed to fresh RPMI-1640 with 10 % FBS 24 h before transfection. The mimics and inhibitors were transfected to cells using Lipofectamine 3000 (Invitrogen, Waltham, MA, USA) at a final concentration of 50 nM. The medium was changed again to fresh medium 6 h after transfection.

qRT–PCR analysis

Total RNA was extracted using the TRIzol reagent (Invitrogen), and complementary DNA (cDNA) was synthesized with the PrimeScript RT reagent Kit (TaKaRa, Dalian, China). Accordingly, qRT–PCR analysis was performed in triplicate using the SYBR Premix ExTaq (TaKaRa). The primers used for amplification of genes of interest are listed in Supplementary Table 6. Quantification of EBV-miR-BART8 was conducted with TaqMan microRNA assays (ABI, Shanghai, China). Mature miRNAs were reverse transcribed, and qRT–PCR was performed using the All-in-One miRNA qRT–PCR Detection Kit (GeneCopoeia, Guangdong, China) following the manufacturer's protocol. RPU6B and β-actin were used for normalizing the expression of miRNA and mRNA, respectively. Fold changes were calculated using the $2^{-\Delta\Delta Cq}$ method.

Plasmid preparation and cell transfection

The GV230 expression vector (http://www.genechem.com.cn) containing the whole coding sequence of *PAG1*, and HA-vimentin, as well as the GV170 control vector were purchased from GeneChem (Shanghai, China). Plasmid DNAs were purified using the TIANprep Mini Plasmid Kit (TIANGEN, Beijing, China) and transduced into NPC cells following the manufacturer's instructions.

RNA Sequencing

RNA-deep sequencing was performed and analyzed in Aksomics, Inc, Shanghai, China. In brief, mRNAs were isolated from DNase-treated total RNA using the Dynabeads mRNA Purification Kit (Invitrogen) . According to the manufacturer's instructions, mRNAs were fragmented with divalent cations and converted to single-stranded cDNA using random hexamer primers and Superscript II reverse transcriptase (Invitrogen). The second strand of cDNA was generated by RNase H (Enzymatics,Beverly, MA,USA) and DNA polymerase (Enzymatics). Subsequently, cDNA products were purified using Ampure beads XP (Beckman, Indianapolis, IN, USA). After converting the overhangs into blunt ends using the T4 and Klenow DNA polymerases (Enzymatics), an extra "A" base was added to the 3'-end of cDNA by the Klenow enzyme. Sequencing adapters were then ligated to the end of cDNA by T4 DNA Ligase (Enzymatics). Fragments of 200 bp were selected using Ampure beads XP (Beckman) and enriched through 12 cycles of PCR. PCR products were loaded into a flowcell to generate clusters and then sequenced using the Hiseq 2000 system (Illumina). Selected results are shown in Supplementary Table 7.

MiRNA target predictions

EBV-miR-BART8 candidate targets were initially obtained from the RNA sequencing results (Supplementary Table 7) and then enriched through literature retrieval (Supplementary Table 8). The RNAhybrid program (http://bibiserv.techfak.uni-bielefeld.de/rnahybrid/submission. html) was used to predict the duplex complementation between the human *PAG1* 3'-UTR and miR-BART8-3p.

Luciferase reporter assays

The MiTarget microRNA 3'-UTR target vector (pEZX-MT01, Gene) containing the full-length 3'-UTR of *PAG1* with binding sites for EBV-miR-BART8-3p (wild-type 3'-UTR) was provided by GeneCopoeia. The mutant site in *PAG1* 3'-UTR was then generated by site-directed mutagenesis using the KOD-Plus-Mutagenesis Kit (SMK-101, Toyobo C. Ltd, Life Science Department, OSAKA, JAPAN). For luciferase reporter assays, the wild type (wt) or mutant (mut) 3'-UTR vector was cotransfected with EBV-miR-BART8-3p mimic or nonspecific mimic control (Genepharma) into HEK 293T cells, respectively. Luciferase activity was measured 48 h after transfection using the Luc-Pair miR Luciferase Assay Kit (GeneCopoeia) on a Panomics Luminometer (Panomics Inc. Fremont, CA, USA).

Co-immunoprecipitation and mass spectrometry assays

To determine potential PAG1-binding proteins, HONE1 and 5-8F cells transfected with the empty vector, as well as flag-PAG1-expressing HONE1 and 5-8F cells were used for coIP employing anti-flag beads. The PAG1 protein complex was eluted using a 0.1 M blycine solution (Fude), separated on an SDS gel, visualized by silver staining using the silver staining kit (Invitrogen), and analyzed by MS at Genepharma (Supplementary Table 9). CoIP assays were performed using 1 mg cell lysates in NP-40 buffer (Fude), with anti-HA and anti-Flag antibodies being employed to pull down the PAG1 and vimentin protein, respectively.

Ethical statement

This study was reviewed and approved by the Ethics Committee of Nanfang Hospital, Southern Medical University (Guangzhou, Guangdong, China) and was conducted in accordance with the Declaration of Helsinki.

Statistical analysis

All experiments were performed in triplicate. Data shown are mean ± s.e.m. (unless otherwise specified), from at least 3 independent experiments. The SPSS 16.0 software (IBM SPSS Statistics, Chicago, IL, USA) was used for statistical analyses. Differences were considered to be statistically significant at values of $P < 0.05$ by Student's *t*-test or χ^2 test (categorical variables) for 2 groups, or by one-way ANOVA (analysis of variance) analysis for multiple groups. Correlations were analyzed using the two-tailed Spearman's correlation analysis. Single, double, and triple asterisks indicate statistical significance *P < 0.05, **P < 0.01, and ***P < 0.001.

Results

Epstein–Barr virus (EBV)-positive radioresistant nasopharyngeal carcinoma cells promoted metastasis

Recurrence of NPC has often been associated with radiotherapy resistance. Metastasis is a significant characteristic of the recurrence of NPC. Based on preliminary analysis of clinical samples, we found that the metastasis rate of patients with recurrent NPC was much higher than that of patients with primary NPC (Supplementary Figure 1). To explore the correlation between metastasis and radioresistance, we generated an acquired radioresistant NPC cell line, termed C666-1R. The radioresistance of this cell line was verified by colony formation assay (Fig. 1A and 1B). Moreover, we used transwell and Boyden assays to detect the migration and invasion ability of C666-1R cells. These assays showed that C666-1R cells had a more visible migration and invasion ability than C666-1 cells, which was confirmed by quantitative analysis (Fig. 1C). In addition, we generated a tumor model in nude mice through Caudal vein injection of C666-1R and C666-1 cells. On day 14, live-animal imaging technology and observation of major organs (lungs and liver) revealed the occurrence of more obvious metastasis in the C666-1R group. The results of the histologic evaluation and statistical results from different groups are shown in Figure 1D-G. The above in vitro and in vivo experiments confirmed that radioresistant NPC cells exhibited stronger invasion and metastasis ability.

Epstein–Barr virus (EBV)-encoded miR-BART8-3p impelled the migration, invasion, and epithelial-mesenchymal transition of nasopharyngeal carcinoma cells

In order to explore the mechanism of radiotherapy resistance promoting metastasis of NPC, we detected the expression level of miRNAs in C666-1R cells and discovered the increased expression of miR-BART8-3p (Supplementary Figure 2). In previous studies, we found that the EBV-encoded miRNA-BART8-3p was closely related to the radioresistance of NPC. Next, we explored whether miRNA-BART8-3p might also play a role in invasion and migration. Respectively, we generated miR-BART8-3p transfected cell lines using the 5-8F and HONE1 EBV-negative NPC cell lines (EBV products, including miRNA-BARTs are not encoded) (Supplementary Figure 3). Wound-healing and transwell assays demonstrated that upregulation of miR-BART8-3p dramatically increased the ability of either 5-8F-BART8 (6 h, $p<0.001$, 12h, $p<0.001$) or HONE1-BART8 (12 h, $p<0.05$, 24h, $p<0.001$) cells for migration compared with the relative control (Fig. 2A). Boyden assays revealed that the upregulation of miR-BART8-3p significantly increased the ability for cell invasion (Fig. 2B-C). To verify these results, we downregulated the expression of miR-BART8-3p in HNE1-EBV and 5-8F-BART8-3p cells through transfection with BART8-inhibitory oligonucleotides. Consistent with the upregulation results, downregulation of miR-BART8-3p by in-BART8-3p was observed to dramatically decrease the migration and invasion abilities of cells (Supplementary Figure 4-7). In addition, we noted a change in cell morphology under microscopic observation, following the transfection of 5-8F and HONE1 cells with miR-BART8-3p; the key characteristics of EMT are known to include a morphological change from a cobblestone-like epithelial appearance to an elongated, spindle-like fibroblastic shape (Fig. 2D). This phenomenon led us to further explore the effect of miR-BART8-3p on EMT of NPC cells. Besides the morphological change, other important features of EMT are known to

include cytoskeletal reorganization, cadherin switching involving downregulation of epithelial E-cadherin and upregulation of mesenchymal N-cadherin, enhanced resistance to cell death, and acquisition of a migratory phenotype. Accordingly, we detected the cadherin switching and our results further showed that miR-BART8-3p increased the RNA and protein levels of stromal markers (N-cadherin, vimentin) and decreased those of the epithelial marker (E-cadherin) (Fig. 2E-F). We observed stained NPC cells using confocal microscopy and clearly observed the position of E-cadherin and vimentin (Fig. 2G). These results suggested that miR-BART8-3p regulates the migration, invasion, and EMT of NPC cells.

Epstein–Barr virus (EBV)-encoded miR-BART8-3p directly targeted *PAG1* in nasopharyngeal carcinoma cells

To further reveal the mechanism of the miR-BART8-3p regulation of NPC metastasis, we compared the gene expression profiling of HONE1-BART8-3p versus HONE1-NC cells employing RNA-sequencing analysis. Our results identified 692 downregulated genes, from which many metastasis-associated candidates could be retrieved (Fig. 3A). Previous studies reported that the VHOT algorithm could predict 112 genes directly targeted by miR-BART8-3p (Supplementary Table 8). Combined with the above 2 methods, we screened out the potential target gene *PAG1* (Fig. 3B). To clarify whether *PAG1* was a direct cellular target for miR-BART8-3p, we performed luciferase reporter assays by cotransfection of a wild-type (WT) or mutant (MUT) *PAG1* 3'-UTR-containing luciferase reporter vector with a miR-BART8-3p mimic. The luciferase activity of the WT *PAG1* 3'-UTR, but not that of the MUT 3'-UTR was shown to be significantly reduced by the BART8-3p mimic (Fig. 3C-D).Concomitantly, we found that the expression level of *PAG1* was decreased in NPC cells and radioresistant cells (Fig. 3E-F). Further evaluation of the regulatory effect of miR-BART8-3p on *PAG1* showed that upregulation of miR-BART8-3p resulted in significant downregulation of *PAG1* at both the RNA and protein levels (Fig. 3G-H). The above results suggested that miR-BART8-3p could regulate *PAG1* in both structure and composition. To verify the plausibility of this conclusion, we reexamined the expression levels of *PAG1* in patient tissues using IHC and observed a significant decrease in the expression of *PAG1* in NPC tissues compared with NP tissues (Fig. 3I).

PAG1 regulated radioresistance and metastasis of nasopharyngeal carcinoma cells

To study the correlation between *PAG1* and the radioresistance or metastasis of NPC, we transfected a PAG1 expression vector into HOEN1 and 5-8F cells. Increased expression of *PAG1* was shown to significantly increase the radiosensitivity of the cell lines (Fig. 4A). Besides, we transfected a PAG1 small interfering RNA plasmid vector into HOEN1 and 5-8F cells (supplementary figure 8), which was observed to lead to the increased migration and invasion of both HOEN1-siPAG1 and 5-8F-siPAG1 cells compared with those induced by the relative siPAG1 plasmid control (Fig. 4B-C). Likewise, EMT related detection revealed that siPAG1 increased the levels of stromal markers, whereas decreased those of epithelial markers (Fig. 4D-F). These results suggested that *PAG1* regulates the radioresistance and metastasis of NPC cells.

PAG1 interacted with vimentin

To further investigate the underlying mechanism by which PAG1 promoted NPC migration and metastasis, we performed an immunoprecipitation assay followed by mass spectrometry to identify PAG1-interacting proteins (Fig. 5A). Respectively, we found vimentin as one of the potential PAG1-interacting proteins from a list of identified proteins, and our coIP assay verified the correlation between PAG1 and vimentin (Fig. 5B). Immunoprecipitation of endogenous PAG1 resulted in the detection of the presence of vimentin, with the reciprocal performed coIP also confirming the correlation between PAG1 and vimentin (Fig. 5B). In addition, we clearly observed the colocalization of PAG1 with HA-vimentin, but not HA alone, in HA-vimentin transfected cells, under the same conditions (Fig. 5C), which further confirmed the combination of PAG1 and vimentin in NPC cells.

Epstein–Barr virus (EBV)-miR-BART8-3p promoted metastasis of nasopharyngeal carcinoma cells in vivo.

In order to evaluate the necessity of PAG1 in the regulatory mechanism of miR-BART8-3p, we restituted the expression of *PAG1*, and found that it significantly reduced the migration, invasion, and EMT phenotypic transformation of 5-8F-BART8-3p cells compared with those induced by the relative PAG1-negative plasmid control (Fig. 6A-D). Considering that overexpression of miR-BART8-3p in EBV-negative NPC cells did not accurately simulate the pathogenesis, we further used EBV-positive NPC cells for validation (Fig. 6A-D). So, we came to the conclusion that restored PAG1 could rescue the phenotypes produced by miR-BART8-3p. Then, we xenografted 5-8F-BART8-3p cells into the caudal vein of nude mice. Upregulation of miR-BART8-3p was demonstrated to significantly increase the metastasis in liver and lungs compared with the 5-8F-NC (Fig. 6E-H), in which miR-BART8-3p was shown to promote the metastasis of NPC.

Epstein–Barr virus (EBV)-miR-BART8-3p and PAG1 were independent prognostic factors for the clinical outcome in patients with nasopharyngeal carcinoma, respectively

To investigate whether the expression of miR-BART8-3p might be associated with clinicopathologic features of NPC, we determined the expression of miR-BART8-3p in a cohort of 82 NPC samples with known TNM-stage (Fig. 7A). The expression of miR-BART8-3p was shown to be dramatically increased in N2–3 as compared with N0–1 stages. Similarly, a substantial higher level of miR-BART8-3p was observed in advanced clinical stage III–IV compared with early clinical stage I–II (Fig. 7A). Thus, these results suggested that EBV-encoded miR-BART8 might contribute to the metastasis of NPC. Using IHC, we further determined the expression of *PAG1* in another cohort of 111 NPC samples with known TNM-stage. The expression of PAG1 was observed to be decreased in M1 as compared with M0 stages. Similarly, a substantial lower level of PAG1 was observed in advanced clinical stage III–IV relative to early clinical stage I–II. Besides, the expression level of PAG1 was shown to be lower in advanced than primary NPC (Fig. 7B-C). Among the 110 patients, the 5-y overall (OS), progression-free (PFS), local relapse-free (LRFS), and distant metastasis-free (DMFS) survival were observed to be significantly improved in the PAG1 high expression group compared with the PAG1 low expression group (Fig. 7B–E). In summary, PAG1 was demonstrated to be closely related to the clinical prognosis in NPC.

Discussion

In this study, we observed that radioresistant NPC cells exhibited a greater tendency for metastasis than radiosensitive NPC cells. In order to find the crux factor for this problem, we tested the expression of EBV-encoded miRNAs in radioresistant or radiosensitive C666-1 NPC cells and found that the expression of miR-BART8-3p was significantly increased in these cells. More specifically, miR-BART8-3p could promote the invasion, metastasis, and EMT of NPC cells by targeting and inhibiting the *PAG1* host gene, which combined with vimentin targets the activity of skeleton proteins and might thus affect their regulation and function. Moreover, miR-BART8-3p and PAG1 were closely related to TNM stages and survival, suggesting that they are important prognostic factors in NPC.

The principal obstacle to long-term survival after NPC radiotherapy is radioresistance. It is noteworthy that the rate of metastasis in patients with recurrent NPC is significantly higher than that in patients with primary NPC. The pathogenesis of this process remains uncertain. We conducted analysis of clinical samples and in vivo and in vitro functional experiments and demonstrated the phenomenon that radioresistant NPC has a greater tendency to EMT and metastasis. To explore the plausible molecular mechanisms, and whether changes in genes induced by radiotherapy might lead to the improvement of the ability of cells for invasion and metastasis, we screened the EBV-encoded miRNA BART8-3p identified from the table of differences between radiosensitive and radioresistant NPC cells. The miR-BART8-3p is known to target the *PAG1* host gene in NPC and regulate the mutual binding of PAG1 and vimentin, partly explaining the enhanced ability for invasion and metastasis caused by radioresistance. However, there are often 2 sides to an issue. An increasing number of studies have suggested that EMT or EMT-factors represent a critical process affecting the DNA damage response (DDR)-mediated sensitivity of cancer cells to radiotherapy and chemotherapy [8-10]. For instance, the Snail, Slug, and *ZEB1* EMT-factors were determined to be DNA repair regulators of radiotherapy and chemoresistance in colorectal, bladder cancer, and so on [11-14] Further studies are needed to discover various other mechanisms connecting EMT and radioresistance.

Infection by EBV is the most important characteristic in NPC. EBV-encoded miRNA BARTs have been reported to regulate several functions by targeting and regulating host genes. Our team has been focusing on the functional and clinical significance of EBV-encoded BARTs, but so far has focused on the single aspect of the treatment of resistance or metastasis. Based on these reports, both EBV-miR-BART1, and EBV-miR-BART7-3p have been shown to induce tumor metastasis by regulating various kinds of pathways in NPC [7, 15]. We further discovered that EBV-miR-BART7-3p increased the chemoresistance of NPC [16]. With the development of the research of BARTs, we began to explore the bridge between the treatment of resistance and metastasis. Studies have shown that 52 % of NPC demonstrated high level expression of EBV-miR-BART8-3p and could induce EMT, promoting the metastasis of cells [17], which was consistent with our results. In our previously reported study, we found that the EBV-encoded miRNA BART8-3p promoted radioresistance in nasopharyngeal carcinoma by regulating the ATM/ATR signaling pathway [18]. In this study, we combined radioresistance with metastasis and found that radioresistant NPC cells were characterized by the overexpression of miR-BART8-3p , promoting PAG1-dependent EMT

and metastasis. These primary study results suggested that radioresistant NPC cells have a stronger ability for metastasis due to a gene advantage. In addition to the positive effect of radioresistance on metastasis, we also preliminary observed the reverse trend of the effect of metastasis to radioresistance. In our evaluation of the EMT status of NPC cells, we noticed that changes in *ZEB1* were associated with EBV-miR-BART8-3p and *PAG1* and further detected that the expression of *ZEB1* was exhibiting a positive correlation with radioresistance or overexpression of miR-BART8-3p, but a negative correlation with PAG1 (Supplementary Figure 9); however, the mechanism needs to be further explored.

The protein encoded by *PAG1* is a type III transmembrane adaptor protein that binds to the tyrosine kinase family of proteins. First, it is thought to be involved in the regulation of the activation of T-cells and mast cells. It has been also reported to regulate the formation of immunological synapses and cell adhesion signaling by preventing the dynamic arrangement of lipid raft proteins. Then, a study found that PAG1 might exhibit ambivalent functions in several carcinomas by interacting with the Src family kinase (SFK), regulating downstream effector pathways [19]. Especially important, upregulation of *PAG1* has been shown to contribute to the promotion of tumor progression and chemoresistance of adipose-derived mesenchymal stem cells in breast cancer [20]. In addition, we also found that the expression of *PAG1* exhibited obvious organizational heterogeneity. Although, high levels of expression of PAG1 has been shown in cancers, such as breast cancer and liver hepatocellular carcinoma, PAG1 has been reported to exhibit low expression in lung squamous cell carcinoma and rectum adenocarcinoma (Supplementary Figure 10). A recent research study suggested that PAG1 might be associated with radioresistance, promoting the inherent radioresistance of laryngeal cancer cells via activation of STAT3 or interaction with integrin β1 [21, 22]. At present, the expression and function of PAG1 in NPC remains unclear. In this study, we found that the expression of PAG1 was negative correlated with the status of patients with NPC, especially the recurrence of NPC. In terms of its function and mechanism, we found that PAG1 binds to the vimentin protein, which is an EMT-related cytoskeletal protein, and inhibits the invasion, migration, and EMT of NPC cells. Besides, overexpression of *PAG1* promoted the radiosensitivity of NPC cells. Based on the analysis of clinical data, we found the OS, PFS, LRFS, and DMFS were significantly improved in the low PAG1-expressing group compared with the high PAG1-expressing group. So, we will continue to explore the role of PAG1 in the DNA repair process (intrinsic radioresistance) and metastasis-associated radioresistance in NPC.

Conclusions

In summary, we demonstrated a correlation between radioresistance and metastasis in NPC, which depended on the elevated levels of the EBV-encoded miRNA BART8-3p. Additionally, we also found that miR-BART8-3p promoted EMT and metastasis of NPC by targeting the inhibition of the *PAG1* host gene. Overall, our findings indicated that high expression of miR-BART8-3p and low expression of PAG1 predicted a poor clinical outcome, and thus could be exploited as critical targets for the development of new therapeutic strategies for the treatment of NPC.

Abbreviations

Co-IP Coimmunoprecipitation

EBV Epstein-Barr virus

EMT epithelial-mesenchymal transition

EBV-miR-BART8-3p EBV encoded miRNA BART8-3p

NPC Nasopharyngeal carcinoma

NP normal nasopharyngeal

rNPC recurrent NPC

siRNA Small interfering RNA

PAG1 Phosphoprotein Associated With Glycosphingolipid-Enriched Microdomains1

DMEM Dulbeccos modified eagle medium

FBS Fetal bovine serum

PBS Phosphate Buffered Saline

EDTA Ethylenediaminetetraacetic acid

PVDF Polyvinylidene fluoride

TBST Tris-Buffered Saline Tween-20

DEPC Diethy pyrocarbonate

FACS Facial action coding system

Declarations

Acknowledgements

Not applicable.

Funding

This work was supported by the National natural Science Foundation of China (81602530, 81773111), Outstanding Youths Development Scheme of Nanfang Hospital, Southern Medical University(2017J004)

Availability of data and materials

Data sharing not applicable to this article as no datasets were generated or analyzed during the current study.

Authors' contributions

XZ, DW and LC were responsible for the design of the study. XZ, YL and YC performed the experiments. YL and YC collected tissue samples. XZ, and LC wrote the first draft of the manuscript. All authors commented on the manuscript and approved the final version.

Ethics approval and consent to participate

The study on NPC cancer samples was approved and supervised by the Research Ethics Committee of Nanfang Hospital of Southern Medical University. Written Informed Consents were obtained from all patients. The animal experiments were performed in strict accordance with the guidelines of the Research Animal Care Committee of Nanfang Hospital of Southern Medical University.

Consent for publication

Not applicable.

Competing interests

The authors declare that they have no competing interests.

References

1. Chen YP, Chan A, Le QT, Blanchard P, Sun Y, Ma J: Nasopharyngeal carcinoma. *LANCET* 2019.
2. Lee AW, Law SC, Foo W, Poon YF, Cheung FK, Chan DK, Tung SY, Thaw M, Ho JH. Retrospective analysis of patients with nasopharyngeal carcinoma treated during 1976–1985: survival after local recurrence. Int J Radiat Oncol Biol Phys. 1993;26(5):773–82.
3. Chua ML, Wee JT, Hui EP, Chan AT. Nasopharyngeal carcinoma. LANCET. 2016;387(10022):1012–24.
4. Lee AW, Ng WT, Chan LK, Chan OS, Hung WM, Chan CC, Cheng PT, Sze H, Lam TS, Yau TK. The strength/weakness of the AJCC/UICC staging system (7th edition) for nasopharyngeal cancer and suggestions for future improvement. ORAL ONCOL. 2012;48(10):1007–13.
5. Karam I, Huang SH, McNiven A, Su J, Xu W, Waldron J, Bayley AJ, Kim J, Cho J, Ringash J, et al: Outcomes after reirradiation for recurrent nasopharyngeal carcinoma: North American experience. *Head Neck* 2015.
6. Hui EP, Li WF, Ma BB, Lam W, Chan K, Mo F, Ai QH, King AD, Wong CH, Guo R, et al: Integrating post-radiotherapy plasma Epstein-Barr virus DNA and TNM stage for risk stratification of nasopharyngeal carcinoma to adjuvant therapy. *ANN ONCOL* 2020.

7. Cai L, Ye Y, Jiang Q, Chen Y, Lyu X, Li J, Wang S, Liu T, Cai H, Yao K, et al. Epstein-Barr virus-encoded microRNA BART1 induces tumour metastasis by regulating PTEN-dependent pathways in nasopharyngeal carcinoma. NAT COMMUN. 2015;6:7353.
8. Zhang P, Wei Y, Wang L, Debeb BG, Yuan Y, Zhang J, Yuan J, Wang M, Chen D, Sun Y, et al. ATM-mediated stabilization of ZEB1 promotes DNA damage response and radioresistance through CHK1. NAT CELL BIOL. 2014;16(9):864–75.
9. Cui Y, Qin L, Tian D, Wang T, Fan L, Zhang P, Wang Z: ZEB1 Promotes Chemoresistance to Cisplatin in Ovarian Cancer Cells by Suppressing SLC3A2. *CHEMOTHERAPY* 2018, 63(5):262–271.
10. Richard G, Dalle S, Monet MA, Ligier M, Boespflug A, Pommier RM, de la Fouchardière A, Perier-Muzet M, Depaepe L, Barnault R, et al. ZEB1-mediated melanoma cell plasticity enhances resistance to MAPK inhibitors. EMBO MOL MED. 2016;8(10):1143–61.
11. Yu JL, Gao X. MicroRNA 1301 inhibits cisplatin resistance in human ovarian cancer cells by regulating EMT and autophagy. Eur Rev Med Pharmacol Sci. 2020;24(4):1688–96.
12. Kowalski-Chauvel A, Modesto A, Gouaze-Andersson V, Baricault L, Gilhodes J, Delmas C, Lemarie A, Toulas C, Cohen-Jonathan-Moyal E, Seva C. Alpha-6 integrin promotes radioresistance of glioblastoma by modulating DNA damage response and the transcription factor Zeb1. CELL DEATH DIS. 2018;9(9):872.
13. Sreekumar R, Emaduddin M, Al-Saihati H, Moutasim K, Chan J, Spampinato M, Bhome R, Yuen HM, Mescoli C, Vitale A, et al. Protein kinase C inhibitors override ZEB1-induced chemoresistance in HCC. CELL DEATH DIS. 2019;10(10):703.
14. Zhong Q, Chen Y, Chen Z. LncRNA MINCR regulates irradiation resistance in nasopharyngeal carcinoma cells via the microRNA-223/ZEB1 axis. *CELL CYCLE* 2019:1–14.
15. Cai LM, Lyu XM, Luo WR, Cui XF, Ye YF, Yuan CC, Peng QX, Wu DH, Liu TF, Wang E, et al. : EBV-miR-BART7-3p promotes the EMT and metastasis of nasopharyngeal carcinoma cells by suppressing the tumor suppressor PTEN. ONCOGENE. 2015;34(17):2156–66.
16. Cai L, Long Y, Chong T, Cai W, Tsang CM, Zhou X, Lin Y, Ding T, Zhou W, Zhao H, et al. EBV-miR-BART7-3p Imposes Stemness in Nasopharyngeal Carcinoma Cells by Suppressing SMAD7. FRONT GENET. 2019;10:939.
17. Lin C, Zong J, Lin W, Wang M, Xu Y, Zhou R, Lin S, Guo Q, Chen H, Ye Y, et al. EBV-miR-BART8-3p induces epithelial-mesenchymal transition and promotes metastasis of nasopharyngeal carcinoma cells through activating NF-κB and Erk1/2 pathways. J Exp Clin Cancer Res. 2018;37(1):283.
18. Zhou X, Zheng J, Tang Y, Lin Y, Wang L, Li Y, Liu C, Wu D. Cai L: EBV encoded miRNA BART8-3p promotes radioresistance in nasopharyngeal carcinoma by regulating ATM/ATR signaling pathway. *Biosci. Rep.* 2019.
19. Fan G, Aleem S, Yang M, Miller WT, Tonks NK. Protein-tyrosine Phosphatase and Kinase Specificity in Regulation of SRC and Breast Tumor Kinase. J BIOL CHEM. 2015;290(26):15934–47.
20. Lu Y, Yang Y, Liu Y, Hao Y, Zhang Y, Hu Y, Jiang L, Gong Y, Wu K, Liu Y. Upregulation of PAG1/Cbp contributes to adipose-derived mesenchymal stem cells promoted tumor progression and

chemoreisitance in breast cancer. *Biochem. Biophys. Res. Commun.* 2017.

21. Dong X, Luo Z, Liu T, Chai J, Ke Q, Shen L. Identification of Integrin β1 as a Novel PAG1-Interacting Protein Involved in the Inherent Radioresistance of Human Laryngeal Carcinoma. J CANCER. 2018;9(22):4128–38.
22. Shen L, Ke Q, Chai J, Zhang C, Qiu L, Peng F, Deng X. Luo Z: PAG1 promotes the inherent radioresistance of laryngeal cancer cells via activation of STAT3. *EXP CELL RES* 2018.

Figures

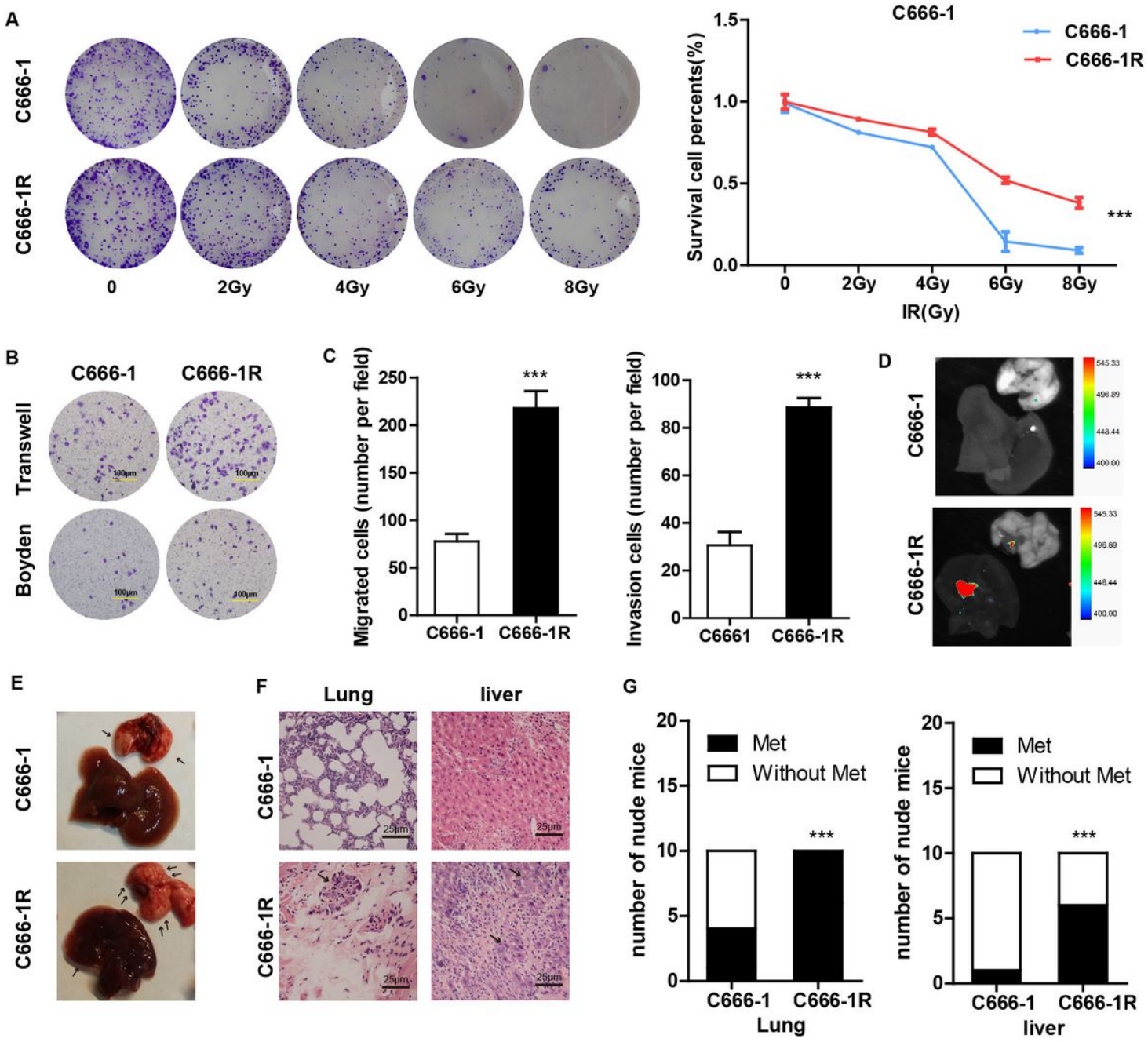

Figure 1

The acquired C666-1R radioresistant cell line showed high invasion and metastasis both in vitro and in vivo. (A) A colony formation assay was performed to assess the radiosensitivity of the C666-1 and C666-1R NPC cells after exposure to 0, 2, 4, 6, or 8 Gy. Cells were cultured for 14 d following irradiation. The differences selected to be compared between the 2 cell lines were detected using repeated measures ANOVA. ***P < 0.001. (B-C) The transwell and Boyden assays revealed different cell motilities among C666-1 and C666-1R cells. Radioresistance clearly promote the migration and invasion of C666-1 cells. Data are presented as the mean ± SEM from 3 independent experiments. ***P < 0.001 by Student's t-test. Scale bar, 100 μm. (D-E) Representative GFP images of tumor metastasis using the LT-9MACIMSYSPLUS whole-body imaging system. Representative GFP and ordinary images of tumor metastasis in organs. The arrow shows the tumor nests. (F) Hematoxylin-eosin staining (H&E stain) shows the lesions in the liver and lungs. The arrow shows the site of the metastatic tumor. Scale bar, 25 μm. (G) Radioresistance increased tumor metastasis in the lungs, and liver. N = 10. Differences were evaluated with the $\chi 2$-test. ***P < 0.001.

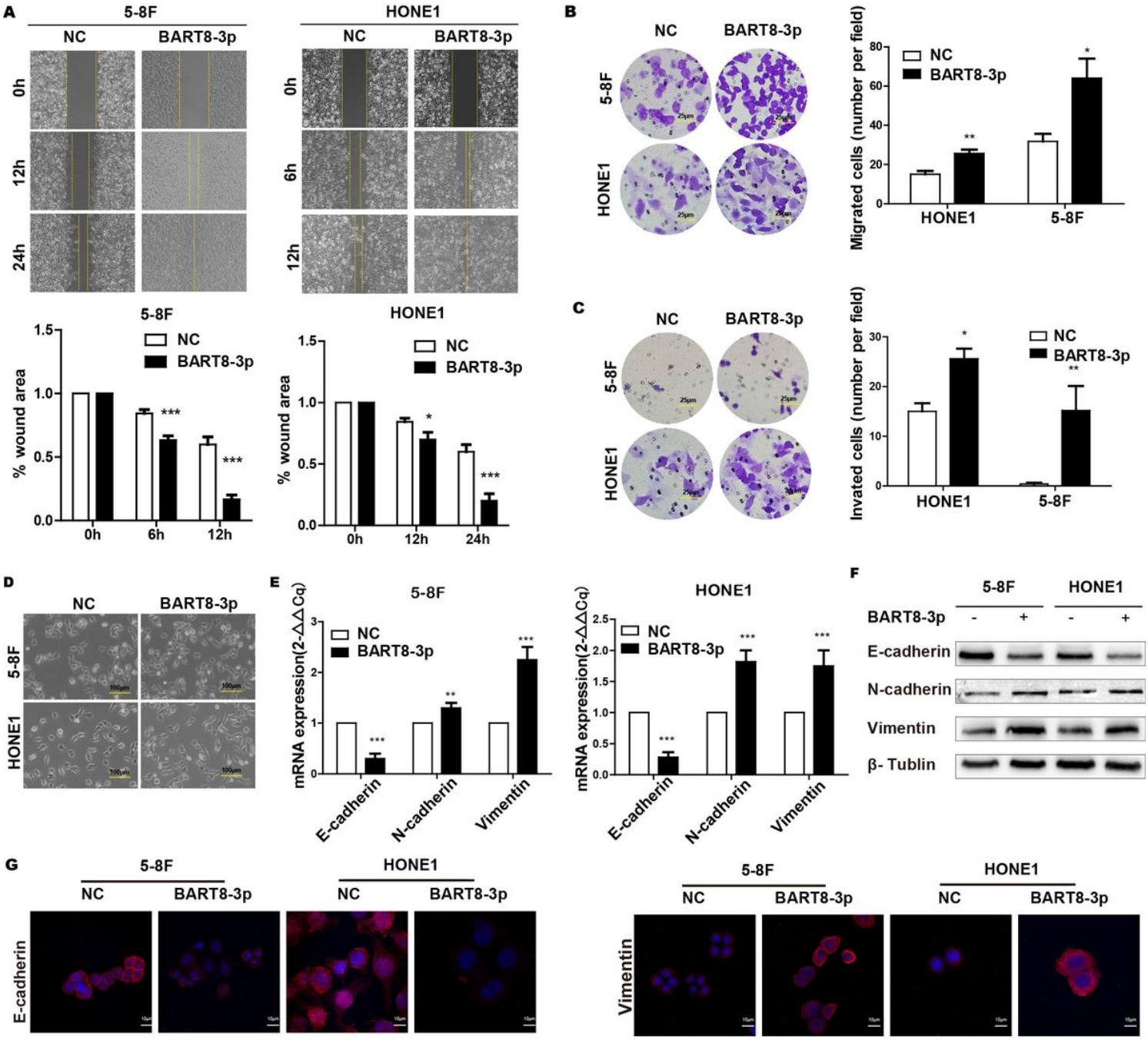

Figure 2

EBV-encoded miRNA BART8-3p promoted the invasion, migration, and EMT of NPC cells (A) Scratch wound-healing assays were conducted in 2 NPC cell lines, HONE1 and 5-8F which following transfection with EBV-miR-BART8-3p, gave rise to the HONE1-BART8-3p and 5-8F-BART8-3p cell lines, respectively. The wound space of HONE1/HONE1-BART8-3p was photographed at 0, 6, and 12 h, whereas that of 5-8F/5-8F-BART8-3p was photographed at 0, 12, and 24 h. Student's t-test. *P < 0.05, ***P < 0.001. (B-C) Upregulation of miR-BART8-3p increased the invasion and migration of both HONE1-BART8-3p and 5-8F-BART8-3p cells. Scale bar, 25 μm. Student's t-test. *P < 0.05, **P < 0.01. (D) Morphology of indicated cells

under phase contrast microscopy. Scale bar, 100 μm. (E-F) The expression of EMT markers was evaluated by qRT-PCR and western blotting. Student's t-test. **P < 0.01, ***P < 0.001. (G) EBV-miR-BART8-3p enhanced EMT. E-cadherin and vimentin were visualized under red fluorescent light. Nuclei were stained with DAPI (blue). Upregulation of BART8-3p modestly increased the expression of vimentin, whereas decreased the expression of E-cadherin. Scale bar, 10 μm.

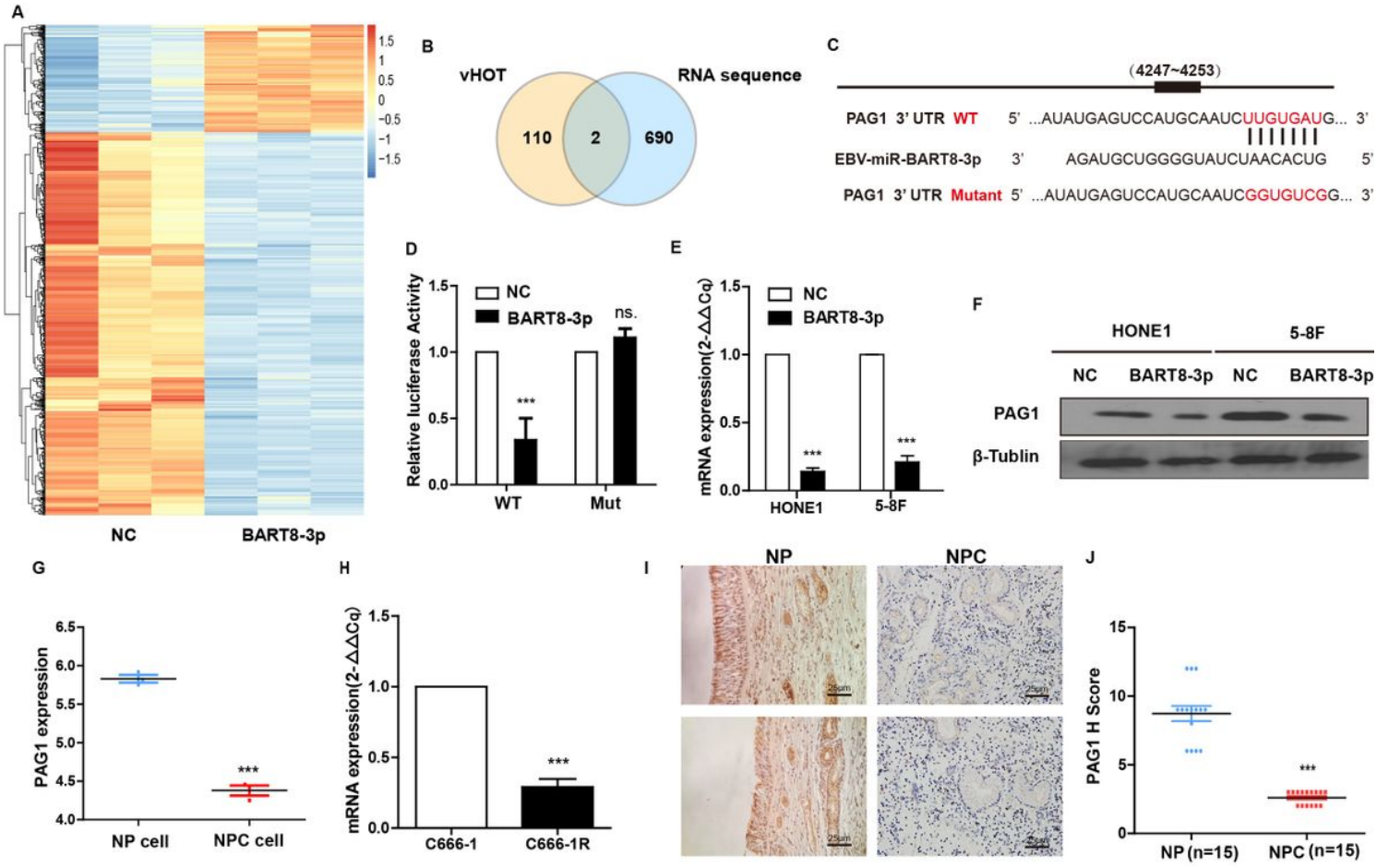

Figure 3

(A) We performed RNA sequencing to find differentially expressed genes between EBV-miR-BART8-3p upregulated and NC HONE1 cells. (B) Development of the vHOT assay and RNA sequencing for the discovery of EBV-miR-BART8-3p targeted genes. (C) Bioinformatics predictions of the BART8-3p binding site in the PAG1 3'-UTR region. Wild-type (WT) and 2 mutant sequences are indicated. (D) Luciferase reporter assays. HEK293T cells were cotransfected with WT or mutated PAG1 3'-UTR along with the BART8-3p mimic or a nonspecific mimic control. The relative repression of the expression of the firefly luciferase was standardized to a transfection control. Student's t-test. ***P < 0.001. (E-F) qRT-PCR and western blotting analysis of the endogenous levels of expression of the PAG1 protein in 5-8F and HONE1 cells treated with EBV-miR-BART8-3p mimic or NC. (G) The mRNA expression level of PAG1 in NPC cells compared with that in nasopharyngeal epithelial (NP) cells. Data were obtained from GSE39826. (H) qRT-PCR was used to measure the levels of the mRNA expression of PAG1 in C666-1 and C666-1R cells. (I-J) Expression of PAG1 in patient samples. The statistical figure represents the representatives of IHC staining for PAG1. Scale bar, 25 μm.

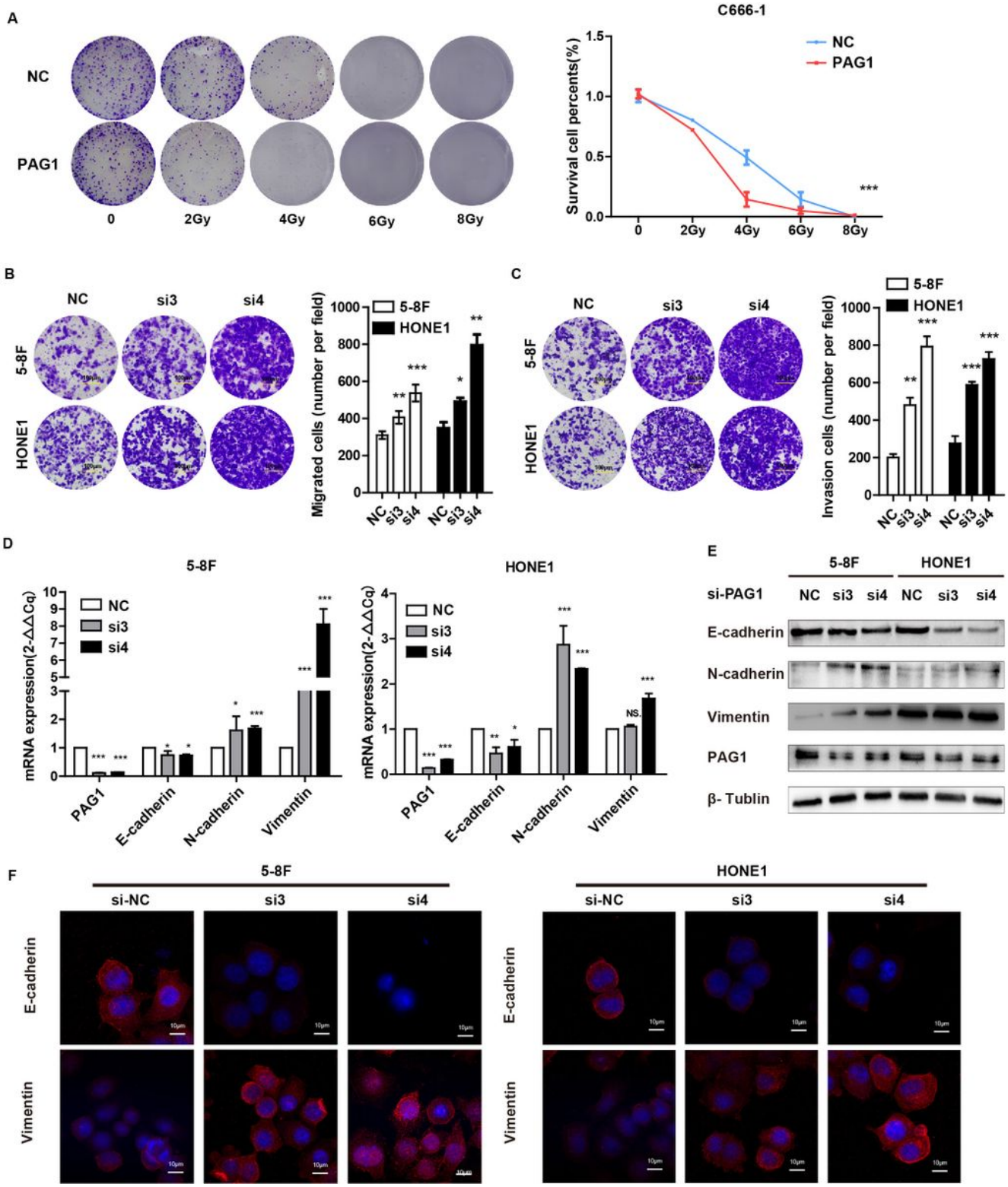

Figure 4

(A) The sensitivity to radiation was tested with colony formation assays in C666-1 cells and PAG1-overexpressing HONE1 cells. (B-C) Transwell assays of HONE1 and 5-8F cells. Following transfection with siPAG1, the migration and invasion of cells was decreased. ***P < 0.0001. Scale bar, 100 μm. (D-F) The expression of EMT markers in indicated cells detected with qRT-PCR, western blotting, and IF assays. NPC cells transfected with siPAG1 show a weaker EMT trend.

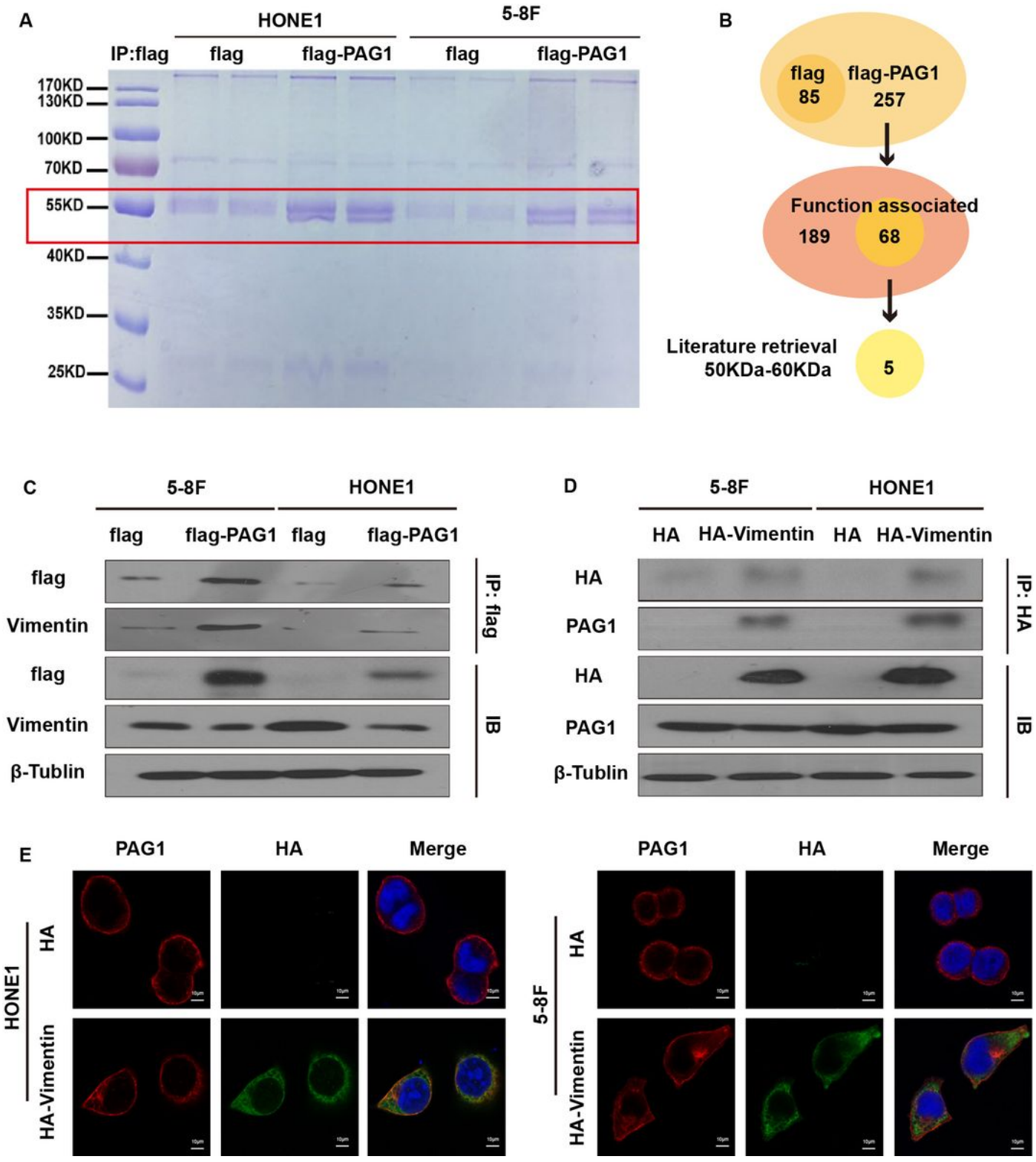

Figure 5

PAG1 specifically binds the EMT-related protein vimentin (A) Immunoprecipitation assay followed by mass spectrometry to identify PAG1-interacting proteins. (B) Schematic represented the selection of PAG1. (C-D) Cell lysates from an NPC cell line treated with a flag-PAG1 or HA-vimentin plasmid were immunoprecipitated (IP) using anti-flag or anti-HA antibodies, followed by immunoblotting (IB) with the indicated antibodies. (E) PAG1 was visualized through red fluorescent labeling in NPC cells, whereas HA-

vimentin was visualized through green fluorescent labeling. Nuclei were stained with DAPI (blue). Red and green fluorescence colocated on the cell membrane. Scale bar, 10 μm.

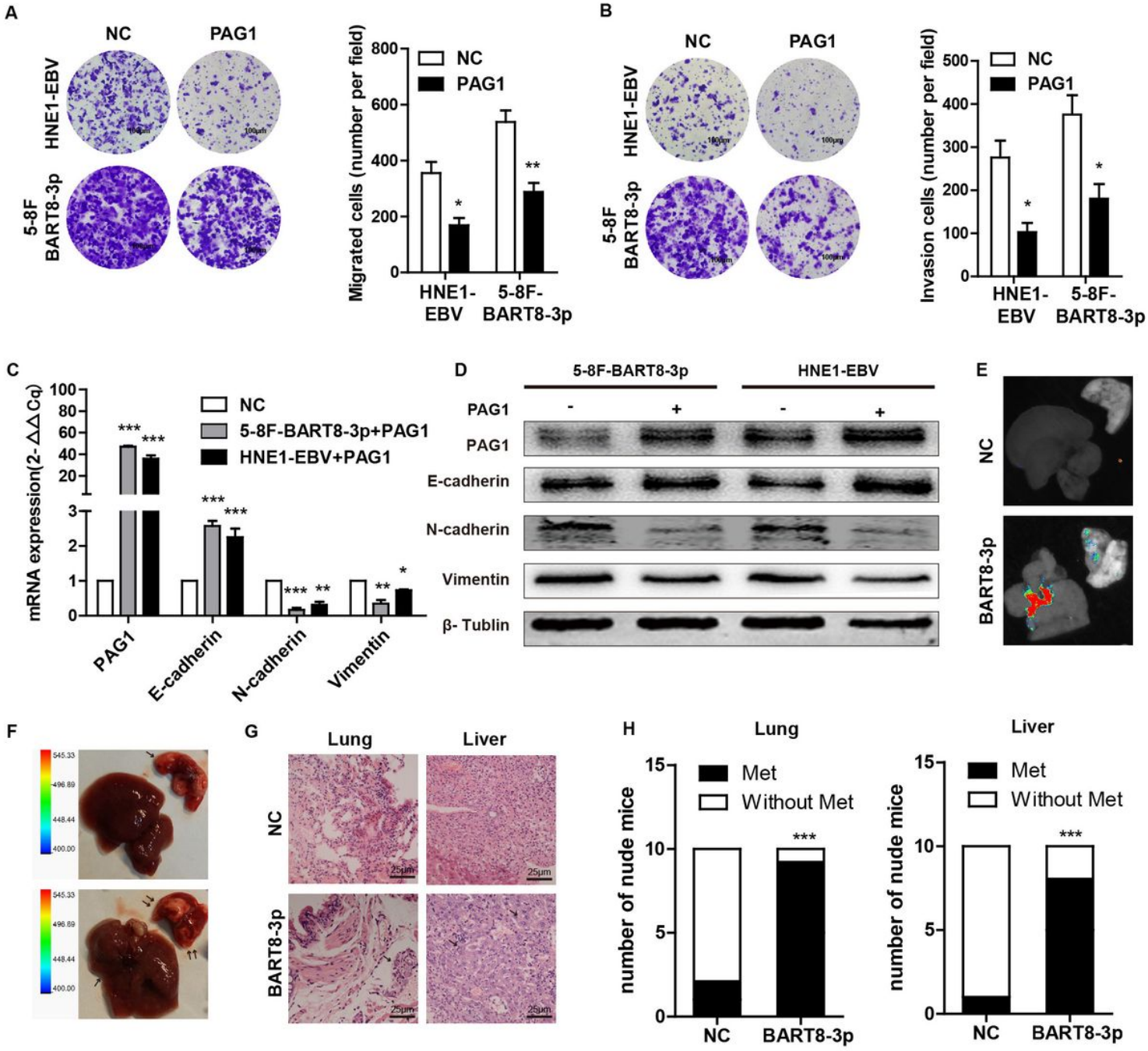

Figure 6

PAG1 reversed the metastasis ability of EBV-miRNA-BART8-3p (A-B) miR-BART8-3p or EBV infection enhances the migration and invasion of NPC cells as determined by transwell and Boyden assays; this effect was reversed following transfection with PAG1. ***P < 0.0001. Scale bar, 50 μm. (C-D) PAG1 reversed the EMT effects induced by miR-BART8-3p or EBV infection in NPC cells. (E-H) Organ imaging. miR-BART8-3p increased tumor metastasis in the lungs, and liver. N = 10. Differences were evaluated with the χ2-test. ***P < 0.001.

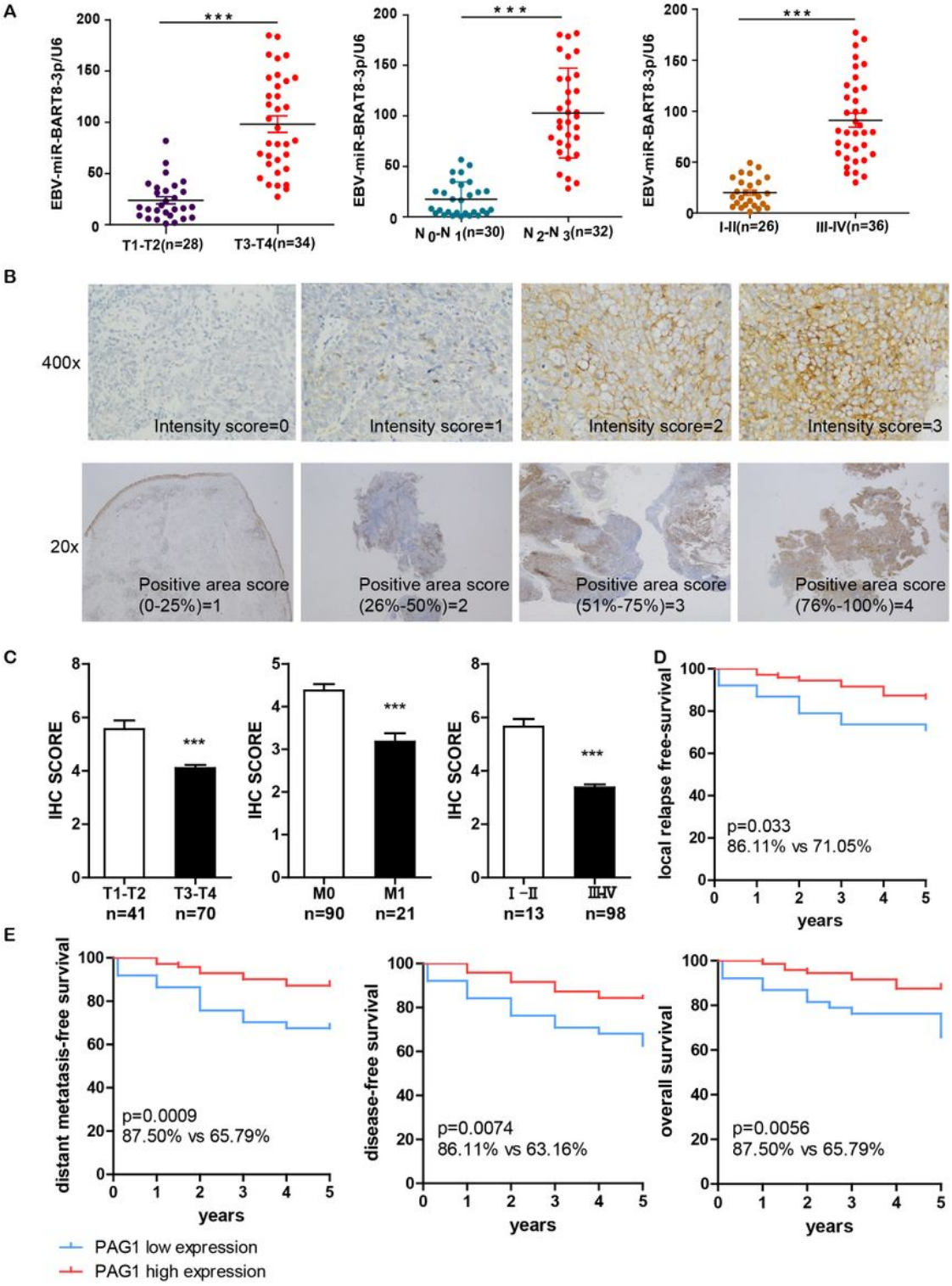

Figure 7

EBV-miRNA-BART8-3p and PAG1 were related to clinical prognosis (A) EBV-miR-BART8-3p was highly expressed in late pathological stages of NPC. The expression of EBV-miR-BART8-3p in a separated cohort of 62 NPC samples was determined by qRT–PCR. RPU6B was used for normalizing the expression of BART1-3p. Student's t-test, ***P < 0.01. (B) Criteria for the intensity scoring of the PAG1 expression. Representative micrographs are shown (×400 and ×20). All micrographs were taken and processed at

identical conditions. (C) PAG1 was lowly expressed in late pathological stages of NPC. The expression of PAG1 in a separated cohort of 62 NPC samples was determined by IHC. Student's t-test, ***P < 0.001. (D-E) Kaplan–Meier analysis of the 5-y locoregional recurrence free (LRFS), distant metastasis-free (DMFS), progression-free (PFS), and overall (OS) survival with regard to the levels of expression of PAG1 in a training set consisting of 111 patients with NPC before initial treatment.

Supplementary Files

This is a list of supplementary files associated with this preprint. Click to download.

- SupplementaryTables.docx
- SupplementaryTables.docx
- supfigures.docx
- supfigures.docx